Journal of Sound and Vibration 527 (2022) 116859

Contents lists available at ScienceDirect

Journal of Sound and Vibration

journal homepage: www.elsevier.com/locate/jsvi

Nonlinear multiple scattering of flexural waves in elastic beams: Frequency conversion and non-reciprocal effects

Angelis Karlos [a,*], Pawel Packo [a], Andrew N. Norris [b]

[a] Department of Robotics and Mechatronics, AGH University of Science and Technology, Al. A. Mickiewicza 30, Krakow, 30-059, Poland
[b] Mechanical and Aerospace Engineering, Rutgers University, Piscataway, NJ, 08854-8058, USA

ARTICLE INFO

Keywords:
Nonlinear multiple scattering
Flexural waves
Frequency conversion
Non-reciprocal scattering

ABSTRACT

Multiple scattering from a cluster of nonlinear point attachments on a beam is formulated and analyzed. The nonlinear equation of motion is solved using a perturbation strategy. The analytical solution is implemented for two common mass–spring–damper systems and for either nonlinear stiffness or nonlinear damping of power-law dependence. The nonlinearity generates harmonic waves at frequencies that are multiples of the incident-wave frequency, and also shifts the linear response of the fundamental frequency. In addition to asymmetric reflection, which is also achievable using linear scatterers with damping, the cluster of nonlinear scatterers can produce asymmetric transmission, thus breaking reciprocity of the system. Analytical results for a single scatterer are presented and validated using Finite Element Method simulations with perfect agreement. A two-scatterer nonlinear cluster acts as a filter that is tunable by the incident amplitude and a three-scatterer cluster that acts as a non-reciprocal frequency converter are considered, demonstrating the potential of the proposed framework for the design of nonlinear scatterer clusters with more complicated scattering properties.

1. Introduction

Clusters of point scatterers of passive linear response attached to a beam can lead to special scattering behavior arising from the interaction of waves reflected and transmitted by each scatterer [1]. An isolated point attachment can be employed to minimize structural vibrations at a single frequency or at a narrow band [2–4]. Such a setup, however, displays a symmetric scattering pattern resulting in an identical response for waves incident from either direction. A cluster of two scatterers is sufficient to obtain non-symmetric, direction-dependent reflection [5] and increased or perfect absorption [5,6]. In the latter case, the asymmetry in reflection properties is obtained by specific distribution of damping properties in the attachments [5]. Despite different reflected wavefields generated upon waves incident from different directions, transmission characteristics remain symmetric in linear passive systems, due to the fundamental principle of reciprocity [7].

Enhanced dynamic performance and specific scattering patterns for a cluster of attachments is possible by employing active control and/or exploiting their nonlinear structural properties. Actively controlled properties of scatterers have been used for adapting the system's response to variable excitation [8] or obtaining broadband performance [9]. Exploiting the nonlinear properties of dynamic systems, on the other hand, offers a certain degree of tunability with no external control system [10]. In particular, wave interaction with nonlinear attachments results in energy redistribution manifesting itself in the generation of other frequency components [10]. It is also well known that waves in nonlinear media display amplitude-dependent dynamic characteristics [11], whose particular features, e.g. intensity and types of harmonic waves, depend on the type of nonlinearity.

* Corresponding author.
E-mail address: angelis.karlos@agh.edu.pl (A. Karlos).

https://doi.org/10.1016/j.jsv.2022.116859
Received 4 August 2021; Received in revised form 18 February 2022; Accepted 19 February 2022
Available online 5 March 2022

Such linear and nonlinear multiple scattering systems are of high practical interest, as these can be used as models to study the dynamics of civil structures, e.g. bridges, offshore floating platforms or runways [12,13] and other, mechanical structures and their components, e.g. structures with cracks [14,15], voids [16], microstructure [17] or mechanical joints, providing an analysis framework for complex nonlinear contact and frictional phenomena [18].

In this article, we exploit the nonlinear properties of the attachment to manipulate mechanical energy flow and analyze their influence on scattering patterns of clusters of attachments. We model an attached element as a passive impedance acting as a point transverse force on a beam. The force consists of a linear interaction of a mass–spring–damper system and an additional contribution of a nonlinear spring and/or damping force. As examples we use cubic dependencies for the force–displacement and force–velocity relations. The nonlinear multiple-scattering problem is converted into a set of inhomogeneous linear multiple-scattering problems, through a perturbation strategy. For this purpose, an expansion of the displacement field is introduced and the resulting sequence of linear inhomogeneous multiple-scattering problems is solved for a single-frequency incident wave, generating scattered waves at both the incident frequency and its odd-integer multiples. The respective frequency components, analogously to the fundamental wave component, undergo multiple-scattering phenomena and result in complex, frequently non-symmetric and non-reciprocal, scattering patterns. The proposed solution approach also indicates that higher-order perturbation problems result in correction terms to the fundamental-frequency wave amplitude and phase and, therefore, predict amplitude dependency of the reflection and transmission properties, and hence amplitude tunability of the system.

We illustrate the complex nonlinear scattering patterns by first describing the properties of a single scatterer, followed by examples of clusters of two and three nonlinear scatterers. In particular, we show that in addition to the non-symmetric reflection, non-symmetric (non-reciprocal) transmission is also possible with nonlinear scatterers. Furthermore, we demonstrate that wave energy can be redistributed to other frequency bands, offering intriguing properties for frequency converters and other acoustic devices. Finally, we note that the described complex dynamic properties are tunable and may be controlled by changing the incident wave amplitude.

The paper is structured as follows. The nonlinear multiple-scattering problem is formulated and solved in Section 2, leading to the derivation of the reflection and transmission coefficients for different harmonic wave components. Results from analytical formulas and numerical simulations are presented in Section 3, illustrating the particular scattering properties introduced by the nonlinearity. Conclusions are summarized in Section 4.

2. Scattering by multiple nonlinear point attachments

2.1. Nonlinear equations of motion

The beam has bending stiffness $D\ (=EI)$ and mass per unit length ρ'. The scatterers are located at positions x_α, $\alpha = 1, \dots, N$. The transverse displacement $w(x,t)$, a real-valued quantity, satisfies

$$\partial_x^4 w + k^4 \partial_\tau^2 w = \sum_\alpha \hat{f}_\alpha \delta_\alpha, \tag{1}$$

where k is the flexural wavenumber, defined by $k^4 = \omega^2 \rho'/D$, $\tau = \omega t$ is nondimensional time, and ω is the angular frequency. Harmonic time dependence according to $\exp(-\mathrm{i}\omega t)$ is considered throughout this article. From here on we adopt the subscript notation indicating functions evaluated at a specific position, i.e. $\delta_\alpha = \delta(x - x_\alpha)$, $w_\alpha(\tau) = w(x_\alpha, \tau)$ etc. In (1), $\hat{f}_\alpha = \hat{f}_\alpha\left(w_\alpha(\tau), w'_\alpha(\tau)\right)$ is the force of the αth scatterer acting on the beam normalized by D and has units of inverse area, and $w'_\alpha(\tau)$ denotes an additional displacement degree of freedom of the αth scatterer (see e.g. Appendix B). The attachment forces $\hat{f}_\alpha$ consist of two contributions, linear, f_α, and weakly nonlinear, f^*_α,

$$\hat{f}_\alpha = f_\alpha + \epsilon f^*_\alpha, \tag{2}$$

where ϵ is a bookkeeping perturbation parameter and all the forcing terms may depend on w_α and w'_α.

We consider a solution of Eq. (1) by perturbation analysis and introduce an expansion for the displacement field as

$$w(x,\tau) = w_0(x,\tau) + \epsilon w_1(x,\tau) + \epsilon^2 w_2(x,\tau) + \cdots = \sum_{n=0}^{\infty} \epsilon^n w_n(x,\tau), \tag{3}$$

where we require the asymptotic behavior at the scatterers' locations only, since the remaining part of the system is linear. An analogous formula holds for $w'_\alpha(\tau)$. As a consequence, the forcing components assume expansions

$$\hat{f}_\alpha = \sum_{n=0}^{\infty} \epsilon^n f_{n\alpha} + \sum_{n=1}^{\infty} \epsilon^n C_{n\alpha}, \tag{4}$$

where $f_{n\alpha} = f(w_{n\alpha}, w'_{n\alpha})$ and $C_{n\alpha}$ are, respectively, the linear and nonlinear forcing terms at the nth order and αth scatterer. The terms $C_{n\alpha}, n \geq 1$, will depend on the displacement solutions of the previous orders, w_0, w'_0 to w_{n-1}, w'_{n-1}, and their exact form will depend on the scatterer configuration and the type of nonlinearity.

One note regarding the perturbation procedure. The expansion in Eq. (3) assumes $|w_{0\alpha}| \gg |w_{1\alpha}| \gg \dots$, although in certain cases it could be that $w_{0\alpha} = 0$ while $w_{1\alpha} \neq 0$. The expansion of Eq. (4) is really the driving mechanism that produces the displacement of Eq. (3), and in that sense could be considered the main *ansatz*.

Using (3) and (4) in (1) yields

$$\sum_{n=0}^{\infty} \epsilon^n \partial_x^4 w_n + k^4 \sum_{n=0}^{\infty} \epsilon^n \partial_\tau^2 w_n = \sum_{\alpha=1}^{N} \left[\sum_{n=0}^{\infty} \epsilon^n f_{n\alpha} + \sum_{n=1}^{\infty} \epsilon^n C_{n\alpha} \right] \delta_\alpha. \tag{5}$$

Collecting terms of the same powers in ϵ yields a system of equations for the zeroth and higher orders of expansion,

$$\epsilon^0 : \partial_x^4 w_0 + k^4 \partial_\tau^2 w_0 = \sum_\alpha f_{0\alpha} \delta_\alpha, \tag{6a}$$

$$\epsilon^n : \partial_x^4 w_n + k^4 \partial_\tau^2 w_n = \sum_\alpha \left[f_{n\alpha} + C_{n\alpha} \right] \delta_\alpha, \ n \geq 1. \tag{6b}$$

Eq. (6a) describes a classic multiple-scattering problem, while in (6b) additional forcing terms $C_{n\alpha}$ – depending on the previous order solutions – appear. The solution to (6) is therefore obtained sequentially, starting from ϵ^0.

2.2. Linear forcing

We introduce the complex displacement of order ϵ^n at the mth harmonic frequency, $u_n^{(m)}$,

$$w_n(x,\tau) = \frac{1}{2} \sum_{m=1,\dots} u_n^{(m)}(x) e^{-\mathrm{i}m\tau} + \text{c.c.}, \tag{7}$$

where c.c. stands for complex conjugate and the summation is restricted to $m = 1$ for $n = 0$. In the following we assume $m \geq 1$, that is, time-harmonic oscillation. The zero-frequency (DC) component is a special case [19] not considered here. The specific integer values of m depend upon the type of nonlinear forcing considered. Appendix B discusses the particular cases of quadratic and cubic nonlinearity, for which the solutions for m are found sequentially. As noted before, the superscript notation (m) is ignored for the linear case $m = 1$.

The linear forcing term $f_{n\alpha}$ of Eq. (4) is then

$$f_{n\alpha} = \frac{1}{2} \sum_{m=1,\dots} \mu_\alpha^{(m)} u_{n\alpha}^{(m)} e^{-\mathrm{i}m\tau} + \text{c.c.}, \tag{8}$$

where the complex impedance $\mu_\alpha^{(m)}$ is defined by either of the two models described in Appendix A.

2.3. Linear multiple-scattering problem at ϵ^0

We first describe the solution to the zeroth-order problem [5]. The linear force for the $n = 0$ solution follows from Eq. (8) as $f_{0\alpha} = \frac{1}{2}\mu_\alpha u_{0\alpha} e^{-\mathrm{i}\tau} + \text{c.c.}$, where μ_α $(= \mu_\alpha^{(1)})$ depends on the choice of model *A* or model *B* in Appendix A. Using this and (7) in (6a) yields

$$\mathrm{d}_x^4 u_0 - k^4 u_0 = \sum_\alpha \mu_\alpha u_{0\alpha} \delta_\alpha, \tag{9}$$

with the spatial dependence omitted. An analogous equation holds for $\bar{u}_0$, with $\bar{\mu}_\alpha$ instead of μ_α, where the overbar denotes the complex conjugate. The solution to (9) is assumed to be the sum of incident and scattered waves,

$$u_0 = u_0^{\text{inc}} + u_0^{\text{scatt}} = u_0^{\text{inc}} + \sum_\alpha \mu_\alpha u_{0\alpha} g_\alpha, \tag{10}$$

with normalized Green's function $g_\alpha^{(m)}$ of the beam for harmonic $m\omega, m \geq 1$, defined by

$$\mathrm{d}_x^4 g_\alpha^{(m)} - \left(\sqrt{m}k \right)^4 g_\alpha^{(m)} = \delta_\alpha, \tag{11a}$$

$$g_\alpha^{(m)} = g(\sqrt{m}k, x - x_\alpha) = \frac{\mathrm{i}}{4\left(\sqrt{m}k\right)^3} \left(e^{\mathrm{i}\sqrt{m}k|x-x_\alpha|} + \mathrm{i}e^{-\sqrt{m}k|x-x_\alpha|} \right). \tag{11b}$$

The incident wave, u_0^{inc} in Eq. (10) satisfies the corresponding homogeneous version of Eq. (9) (zero right hand side), whereas the scattered wave follows directly from Eq. (9). The complex amplitude is found by solving an $N \times N$ system of linear equations for $\{u_{0\alpha}\}$ obtained by evaluating (10) at the scatterers' locations,

$$u_0(x) = u_0^{\text{inc}}(x) + \sum_{\alpha\beta} u_{0\alpha}^{\text{inc}} \hat{M}_{\alpha\beta}\, g_\beta(x), \tag{12}$$

where $\hat{M}_{\alpha\beta} = \hat{M}_{\alpha\beta}^{(1)}$, and for future reference $\hat{M}_{\alpha\beta}^{(m)}$ are the elements of the inverse of the symmetric matrix with elements

$$M_{\alpha\beta}^{(m)} = \frac{\delta_{\alpha\beta}}{\mu_\alpha^{(m)}} - g_{\alpha\beta}^{(m)}, \tag{13}$$

$\delta_{\alpha\beta}$ is the Kronecker delta and $g_{\alpha\beta}^{(m)} = g_\alpha^{(m)}(x_\beta)$.

2.4. Higher-order multiple-scattering problem at ϵ^n, $n \geq 1$

Extra forcing terms appear at $O(\epsilon^n)$, $n \geq 1$ as compared to the zeroth order, specifically $C_{n\alpha}$ in Eq. (6b). The term $C_{n\alpha}$ can be expressed as a sum of Fourier coefficients $c_{n\alpha}^{(m)}$, whose form will depend on the order of nonlinearity considered (see Appendix B). Expanding the forcing term and the displacements in terms of harmonic components, Eqs. (6b), (7) and (8) give a set of separate equations for the complex amplitudes at frequencies $m\omega$ as

$$\mathrm{d}_x^4 u_n^{(m)} - \left(\sqrt{m}k\right)^4 u_n^{(m)} = \sum_\alpha \left(\mu_\alpha^{(m)} u_{n\alpha}^{(m)} + c_{n\alpha}^{(m)}\right) \delta_\alpha \tag{14}$$

where the complex coefficients $c_{n\alpha}^{(m)}$ are defined in Appendix B. In the following analysis we assume $m \geq 1$, that is, time-harmonic oscillation. The zero-frequency (DC) component forms a special case which is not considered here.

Eq. (14) can be solved analogously to (9), now assuming that the incident wave follows from the nonlinear forcing terms $c_{n\alpha}^{(m)}\delta_\alpha$, which depend on the previous-order solutions and are therefore already calculated. Consequently, the solution to Eq. (14) is

$$u_n^{(m)} = \sum_\alpha g_\alpha^{(m)} \left(\mu_\alpha^{(m)} u_{n\alpha}^{(m)} + c_{n\alpha}^{(m)}\right). \tag{15}$$

As in the case of the leading-order problem, the complex amplitudes are found by solving a system of linear equations,

$$\begin{aligned} u_n^{(m)}(x) &= \sum_{\alpha\beta\gamma} g_\alpha^{(m)}(x) \left(\hat{M}_{\alpha\beta}^{(m)} g_{\beta\gamma}^{(m)} c_{n\gamma}^{(m)} + c_{n\alpha}^{(m)}\right) \\ &= \sum_{\alpha\beta} \frac{c_{n\alpha}^{(m)}}{\mu_\alpha^{(m)}} \hat{M}_{\alpha\beta}^{(m)} g_\beta^{(m)}(x), \end{aligned} \tag{16}$$

with $\hat{M}_{\alpha\beta}^{(m)}$ the inverse of $M_{\alpha\beta}^{(m)}$, as defined previously.

In summary, the full solution for the displacement is

$$w(x,\tau) = \frac{1}{2} u_0(x) e^{-\mathrm{i}\tau} + \frac{1}{2} \sum_{m=1,\ldots} \sum_{n=1}^{\infty} \epsilon^n u_n^{(m)}(x) e^{-\mathrm{i}m\tau} + \mathrm{c.c.} \tag{17}$$

with $u_0(x)$ given by Eq. (12) and $u_n^{(m)}(x)$ by Eq. (16).

2.5. Reflection and transmission coefficients

The nonlinear multiple-scattering problem is expected to be amplitude-dependent. The incident wave at the zeroth order, for left-to-right (+) or right-to-left (−) propagation, is assumed as

$$u_{0\pm}^{\mathrm{inc}} = a\, e^{\pm \mathrm{i}kx}. \tag{18}$$

Following Eq. (10), the leading-order amplitude for waves propagating at either side of the scatterer can be expressed with respect to reflection and transmission coefficients as

$$u_{0\pm}(x) = \begin{cases} u_{0\pm}^{\mathrm{inc}} + aR_{0\pm} e^{\mp \mathrm{i}kx} & \text{for} \quad x \to -\infty, \\ aT_{0\pm} e^{\pm \mathrm{i}kx} & \text{for} \quad x \to +\infty, \end{cases} \tag{19}$$

where [5]

$$R_{0\pm} = \frac{\mathrm{i}}{4k^3} \sum_{\alpha\beta} \hat{M}_{\alpha\beta} e^{\pm \mathrm{i}k(x_\alpha + x_\beta)}, \quad T_{0\pm} = 1 + \frac{\mathrm{i}}{4k^3} \sum_{\alpha\beta} \hat{M}_{\alpha\beta} e^{\pm \mathrm{i}k(x_\alpha - x_\beta)}. \tag{20}$$

As for a linear system, the leading-order reflection coefficients may differ depending on the direction of incidence [5]. The transmission coefficient, however, is independent of incidence, that is, $T_{0+} = T_{0-}$ [5], since the formula $(20)_2$ for $T_{0\pm}$ is symmetric, resulting in reciprocal transmission.

We now deduce the reflection and transmission coefficients of an $m\omega$ harmonic component, generated due to the nonlinearity at expansion order $n \geq 1$, as the complex amplitudes of the harmonics propagating in directions $\mp x$ and $\pm x$, respectively, for incidence towards $\pm x$. We first write the far field at the mth harmonic frequency and order ϵ^n at $x \to \pm\infty$ upon excitation by $u_{0\pm}^{\mathrm{inc}}$ as

$$u_{n\pm}^{(m)}(x)|_{x\to\pm\infty} = a_{n\pm\pm}^{(m)} e^{\pm \mathrm{i}\sqrt{m}kx}, \tag{21}$$

where the first $\pm$ subscript of $a_n^{(m)}$ is the incident wave direction while the second refers to waves scattered towards $x \to \pm\infty$. The two $\pm$ signs in $a_n^{(m)}$ are independent of each other. As a consequence, there are four (possibly different) $a_{n\pm\pm}^{(m)}$ coefficients — two scattered waves for each of the two incident wave directions, which correspond to the appropriate reflection and transmission coefficients as

$$R_{n\pm}^{(m)} = a_{n\pm\mp}^{(m)} = \frac{\mathrm{i}}{4\left(\sqrt{m}k\right)^3} \sum_{\alpha\beta} \frac{c_{n\alpha\pm}^{(m)}}{\mu_\alpha^{(m)}} \hat{M}_{\alpha\beta}^{(m)} e^{\pm \mathrm{i}\sqrt{m}kx_\beta}, \tag{22a}$$

$$T_{n\pm}^{(m)} = a_{n\pm\pm}^{(m)} = \frac{\mathrm{i}}{4\left(\sqrt{m}k\right)^3} \sum_{\alpha\beta} \frac{c_{n\alpha\pm}^{(m)}}{\mu_\alpha^{(m)}} \hat{M}_{\alpha\beta}^{(m)} e^{\mp \mathrm{i}\sqrt{m}kx_\beta}. \tag{22b}$$

It should be noted that the coefficients $R_{n\pm}^{(m)}$ and $T_{n\pm}^{(m)}$ are amplitude-dependent through the amplitude-dependent forcing terms $c_{n\alpha\pm}^{(m)}$. It is apparent that, in general, with nonlinear scatterers both the reflection and transmission coefficients at harmonic frequencies can be different depending on the incidence direction. In particular, it may be seen that in general $R_{n+}^{(m)} \neq R_{n-}^{(m)}$ and $T_{n+}^{(m)} \neq T_{n-}^{(m)}$, so that, apart from non-symmetric reflection, non-reciprocal transmission can also be obtained. Of course, under certain conditions, the reflection and transmission coefficients for different directions of incidence may also coincide, that is, it may be either $R_{n+}^{(m)} = R_{n-}^{(m)}$ or $T_{n+}^{(m)} = T_{n-}^{(m)}$, both of which for example hold for a symmetric cluster of scatterers.

3. Results from simulations

3.1. Computational scheme

The analytical model developed in Section 2 was validated with a nonlinear Finite Element Method (FEM) model. Classical linear two-node four-DOF (two vertical and two rotational) beam elements of length $\Delta x = 0.1$ m have been used for all cases reported later. The model was long enough to avoid end reflections and the cluster was positioned at the center. The excitation was a force applied at the left (or right) end, consisting of a continuous sine wave of a specific frequency (equivalently, wavenumber), with the leading edge profiled by a half-Hanning window in order to minimize energy leakage in the frequency domain. The scatterers were implemented as point force linear and nonlinear sources, following their respective definitions in Appendix A and Appendix B, respectively. The explicit time integration scheme with the second-order central difference was adopted with the time step set to $\Delta t = 0.001$ s to ensure stability. Excitation forces were adjusted to result in desired displacement amplitudes. The single- and multiple-scattering systems were studied for three – arbitrarily selected – amplitudes of $|a| = \{1.00, 1.25, 1.50\} \times 10^{-3}$ m. The linear and nonlinear parameters of the scatterers were selected to satisfy $|w_{0\alpha}| \gg |w_{1\alpha}| \gg \ldots$ in expansion (3). The results were acquired as time–displacement responses at a set of nodes located 50−750 m on the left- and right-hand side of the cluster, to avoid measurement of the near field and end-reflected waves. The acquired waveforms were subsequently postprocessed to compute the transmission, $T^{(1)}$ and $T^{(3)}$, and reflection, $R^{(1)}$ and $R^{(3)}$, coefficients at the fundamental and the third harmonic frequencies.

The transmission coefficients $T^{(1)}$ and $T^{(3)}$ were measured from the Fast Fourier Transform of the spatial profile of the displacement at the opposite side of the scatterer (with respect to the excitation) for a fixed time, at the respective wavenumbers $\{k_{\mathrm{exc}}, \sqrt{3}k_{\mathrm{exc}}\}$. Noting that the incident wave does not contain the third harmonic wave, the reflection coefficient $R^{(3)}$ is computed in the same way, taking the displacement profile of the nodes at the excitation side. The fundamental frequency reflection coefficient, $R^{(1)}$, was computed from the Standing Wave Ratio: $\mathrm{SWR} = \max|w(x)|/\min|w(x)|$, as $|R^{(1)}| = (\mathrm{SWR} - 1)/(\mathrm{SWR} + 1)$, using the total acquired wavefield at the excitation frequency ω. Numerical simulation results, obtained by employing the above-mentioned procedures, are shown in the figures with markers.

In the following sections we present results for two impedance models (see Appendices A and B) and cubic-nonlinear stiffness and damping elements. This particular selection follows from the fact that: (a) a cubic-nonlinear system produces $m = 1, 3$ harmonics at the first order, hence allows the study of higher harmonic wave propagation and results in a correction to the fundamental frequency; also (b) this kind of nonlinearity does not generate the zero-frequency (static offset) component that would make the analysis more complex. For all analytical models, we present results for up to ϵ^2 order.

It should be mentioned that the framework outlined in Section 2 is valid for $|w_{0\alpha}| \gg |w_{1\alpha}| \gg \ldots$ in the expansion, Eq. (3). A violation of this requirement may occur for low-damped cubic-nonlinear scatterers with linear-resonant wavenumber k_n excited by an incident wave at $k_n/\sqrt{3}$, which may cause the third-harmonic response to be greatly amplified. A narrow band around $k_n/\sqrt{3}$ is therefore grayed out in Figs. 3 and 4, where the accuracy of the expansion may require further investigation, which is beyond the scope of this article.

3.2. Single scatterer

3.2.1. Linear reflection and transmission

We consider a single nonlinear scatterer, located at $x = 0$. The reflection and transmission coefficients follow as special cases of Eqs. (20) and (22). In the presence of only one scatterer the linear reflection coefficient is, like the reciprocal linear transmission coefficient, also independent of incidence direction, that is, $R_0 = R_{0\pm}$, as Eqs. (20) reduce to

$$R_0 = \frac{\mathrm{i}\mu}{4k^3 + \mu(1 - \mathrm{i})}, \quad T_0 = 1 + R_0. \tag{23}$$

Equivalently,

$$R_0 = \mathrm{i}e^{\mathrm{i}\phi} \sin\phi, \quad T_0 = e^{\mathrm{i}\phi} \cos\phi, \quad \text{where} \quad \tan\phi = \left(1 + 4k^3/\mu\right)^{-1} \tag{24}$$

with ϕ real in the lossless case (μ real valued), immediately showing energy conservation ($|R_0|^2 + |T_0|^2 = 1$).

The higher-order reflection and transmission coefficients, defined above as farfield amplitudes, are both independent of incidence direction and also coincide with each other, that is, $R_n^{(m)} = T_n^{(m)} = R_{n\pm}^{(m)} = T_{n\pm}^{(m)}$, and are given, as follows from Eqs. (22), by

$$R_n^{(m)} = T_n^{(m)} = (1 + \mathrm{i})^{-1} \left(1/g_0^{(m)} - \mu^{(m)}\right)^{-1} c_{n0}^{(m)}, \tag{25}$$

where $g_0^{(m)} = g\left(\sqrt{m}k, 0\right)$ and $c_{n0}^{(m)} = c_n^{(m)}(0)$. We next present the influence of nonlinear elements on wave propagation.

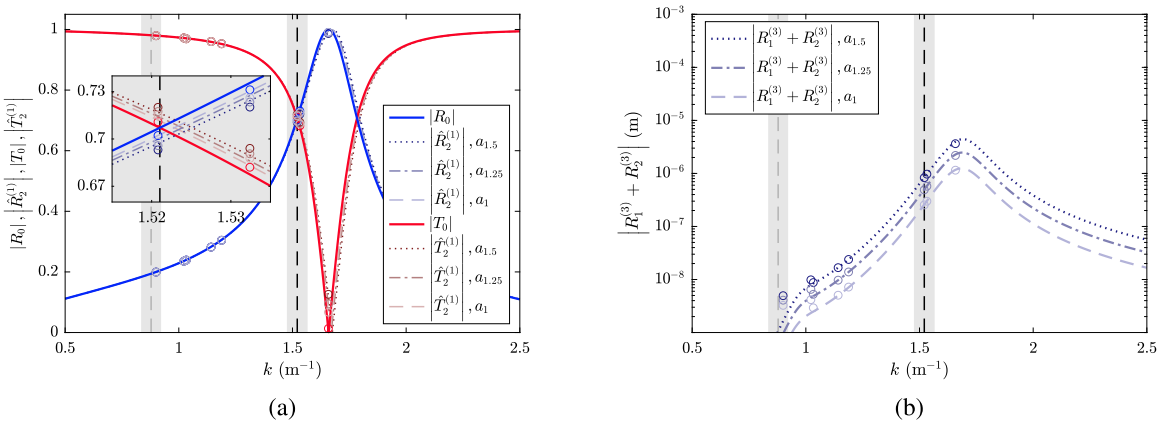

Fig. 1. (a) Leading-order reflection and transmission coefficients for a single scatterer (model A) with cubically nonlinear stiffness, also with higher-order corrections at the fundamental frequency for different incident amplitudes $a_j = j$ mm, $j = 1, 1.25, 1.5$. (b) Reflected amplitudes at the third harmonic for different incident amplitudes. The dashed vertical line corresponds to the linear resonance of the scatterer. The gray patches are centered around $k_n/\sqrt{3}$ and k_n, where $k_n = 1.521$ m^{-1} is the anti-resonance wavenumber of the scatterer. The circles correspond to FEM results.

3.2.2. Single scatterer with nonlinear stiffness, impedance model A

A single scatterer generates harmonics equally towards $\pm x$ regardless of incidence, according to Eq. (25). The equality follows from the spatial symmetry of the Green's function with respect to the scatterer's location and expresses the fact that a single scatterer radiates energy equally in both directions. A lossless scatterer of model A (see Appendix A.1) with the following properties is considered,

$$M = 1 \text{ kg}, \quad \nu = 0 \text{ N m}^{-1} \text{ s}, \quad \kappa = 5.35248 \text{ N m}^{-1}, \quad \kappa^* = 10^4 \text{ N m}^{-3}. \tag{26}$$

Parameters M, ν, κ define the linear impedance via Eq. (A.2) and κ^* defines the cubic nonlinearity, see Appendix B.3. For simplicity it is assumed that $D = 1$ N m^2 and $\rho' = 1$ kg m^{-1} in all simulations.

The reflection and transmission coefficients at the fundamental frequency are plotted in Fig. 1a, both for a linear scatterer, where the coefficients are independent of the incident amplitude, and for a nonlinear scatterer with the properties of Eq. (26), for three different incident amplitudes. For simplicity, the second-order fundamental-frequency reflection and transmission coefficients are represented by $\hat{R}_2^{(1)} = R_0 + \left(R_1^{(1)} + R_2^{(1)}\right)/a$ and $\hat{T}_2^{(1)} = T_0 + \left(T_1^{(1)} + T_2^{(1)}\right)/a$, respectively. Results from FEM simulations are shown with circular markers, also in the following plots for a single scatterer. Bands around both k_n and $k_n/\sqrt{3}$ are grayed-out in all following plots for a single scatterer, where resonances of the fundamental or the third harmonic may cause deterioration of the expansion accuracy, although this requires further analysis. It can be seen that the nonlinearity induces amplitude-dependent shifts to the transmission and reflection coefficients at the fundamental frequency, as can more clearly be observed in the inset of Fig. 1a.

The amplitude of the third harmonic is plotted in Fig. 1b and is seen to be both frequency- and amplitude-dependent, with a characteristic peak slightly above the linear resonance of the scatterer. Good agreement is observed between analytical and numerical results both at the fundamental and at the third harmonic, apart from some discrepancy in the predicted third harmonic at a wavenumber close to $k_n/\sqrt{3}$, within the left grayed-out region in Fig. 1b, although the response is very small there, below 10^{-8} m, which may cause issues of accurately extracting the amplitude numerically in the FEM model.

Two main observations need to be made. First, some portion of the incident wave energy is converted into the third harmonic wave. Second, it can be seen, more clearly in the inset of Fig. 1a, that the nonlinearity causes the reflection and transmission coefficients to shift by different amounts depending on the incident amplitude, thus providing amplitude-dependent tunability, for example of the frequency at which the transmission is zero, or minimum, and the reflection accordingly maximum. Both of these general observations also apply to the other configurations of a single nonlinear scatterer presented below.

3.2.3. Single scatterer with nonlinear damping, impedance model A

Results for a nonlinear scatterer of model A of Appendix A.1 with mass and linear stiffness coefficient as in Eq. (26), but without nonlinear stiffness, that is, $\kappa^* = 0$, and instead with linear damping coefficient $\nu = 0.04627$ N m^{-1} s and nonlinear damping coefficient $\nu^* = 500$ N m^{-3} s^3, are shown in Fig. 2. The same two effects of amplitude-dependent fundamental frequency transmission and reflection can be observed. However, for the case of nonlinear damping, the amplitude–frequency characteristics of the third-harmonic waves are qualitatively different. Namely, although the response peaks occur at the same wavenumbers as with nonlinear stiffness, they are followed by an approximately flat broadband response at higher wavenumbers. The analytical and numerical results match well, apart from some inaccuracies in the FEM-predicted values for the third-harmonic wave when the response is very small, below 10^{-8} m, which again occur at lower k.

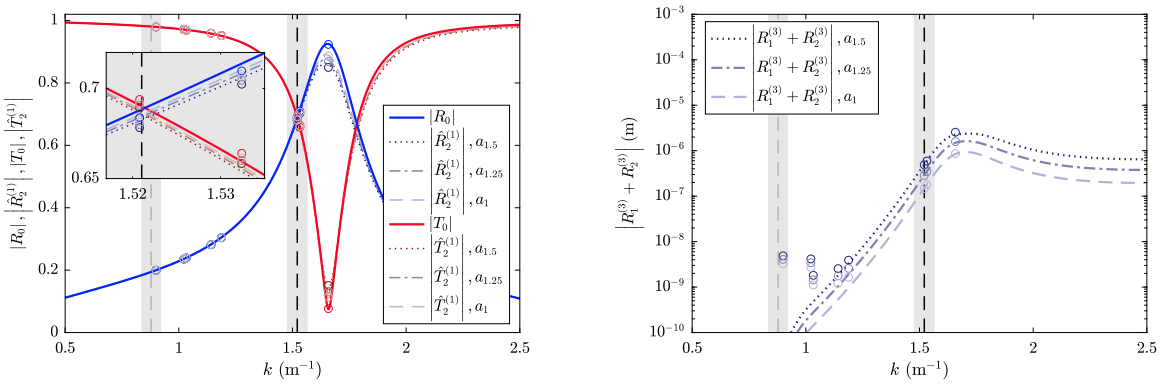

Fig. 2. (a) Leading-order reflection and transmission coefficients for a single scatterer (model *A*) with cubically nonlinear damping, also with higher-order corrections at the fundamental frequency for different incident amplitudes $a_j = j$ mm, $j = 1, 1.25, 1.5$. (b) Reflected amplitudes at the third harmonic for different incident amplitudes. The dashed vertical line corresponds to the resonance of the scatterer. The gray patches are centered around $k_n/\sqrt{3}$, where $k_n = 1.521$ m^{-1} is the anti-resonance wavenumber of the scatterer. The circles correspond to FEM results.

3.2.4. Single scatterer with nonlinear stiffness, impedance model B

A scatterer of model *B* (see Appendix A.2) with the properties of Eq. (26) but with $\kappa^* = 10^5$ N m^{-3} is now considered. The reflection and transmission coefficients at the fundamental frequency are plotted in Fig. 3a, for both the linear and the nonlinear cases for three different incident amplitudes. In the case of a linear scatterer of model *B*, there are two characteristic points, namely, one where the transmission is minimum and the reflection maximum and another with the inverse response, the latter corresponding to the scatterer resonance. Therefore, by varying the incident amplitude, the frequencies at which these characteristic responses occur can be tuned. The generated third harmonic is shown in Fig. 3b for three different amplitudes.

The frequency- and incident-amplitude-dependent third harmonic is plotted in Fig. 3b, and is now seen to have a peak below the linear resonance of the scatterer. It follows from Eqs. (11b), (12), (18), (25), (A.2), (B.6) and $(B.24)_2$ that the dominant contribution to the third harmonic is proportional to the third power of the incident wave amplitude, specifically

$$\begin{aligned} R_1^{(3)} = T_1^{(3)} &= (1+\mathrm{i})^{-1}\left(1/g_0^{(3)} - \mu^{(3)}\right)^{-1}\left(-\frac{\kappa^*}{4D}\right)u_0^3(0) \\ &= \frac{-\mathrm{i}\kappa^* a^3}{16D\left(\sqrt{3}k\right)^3}\left(1+(1-\mathrm{i})\frac{\left(9M\omega^2-\kappa\right)}{4D\left(\sqrt{3}k\right)^3}\right)^{-1}\left(1+(1-\mathrm{i})\frac{\left(M\omega^2-\kappa\right)}{4Dk^3}\right)^{-3}. \end{aligned} \tag{27}$$

This shows that $|R_1^{(3)}| = |T_1^{(3)}| = \mathrm{O}(a^3k^9)$ for $k \ll 1$ and $\mathrm{O}(a^3k^{-7})$ for $k \gg 1$. In this case, the response peak occurs at a wavenumber below resonance. There is excellent agreement between the analytical and numerical models both for the fundamental frequency response and for the generated third harmonic.

3.2.5. Single scatterer with nonlinear damping, impedance model B

A scatterer of model *B* with nonlinear damping is also simulated, with mass and linear stiffness coefficient as in Eq. (26), but with $\nu = 0.04627$ N m^{-1} s, $\kappa^* = 0$ and $\nu^* = 10^4$ N m^{-3} s^3, see Appendix B.3, and the corresponding results are shown in Fig. 4. The expression for the third harmonic reflection coefficient follows from Eqs. (27), (B.6) and (B.26) by the replacement $\kappa^* \to \mathrm{i}\nu^*\omega^3$ in Eq. (27). Hence, $|R_1^{(3)}| = |T_1^{(3)}| = \mathrm{O}(a^3k^{15})$ for $k \ll 1$ and $\mathrm{O}(a^3k^{-1})$ for $k \gg 1$. As for model *A*, the amplitude of the third harmonic generated by the nonlinear damping, plotted in Fig. 4b, remains approximately flat over a broad frequency range beyond the response peak. The analytical and numerical results display excellent agreement, as in the case of nonlinear stiffness for model *B*.

3.3. Multiple scatterers

3.3.1. A tunable filter: amplitude-dependent nearly perfect absorption at the fundamental frequency

A cluster of two scatterers is designed which display amplitude-dependent absorbing properties at the frequency of the incident wave. We assume that the incident wave propagates from left to right, that is, towards $+x$, interacts with the cluster and the response is measured in the forward ($+x$) direction. As a side effect, the cluster generates a third harmonic that propagates towards both sides of the cluster with substantially smaller amplitude-dependency. The starting point for the design is the impedances of a pair of linear scatterers presented in [5] (Eq. (53)), which achieve one-sided total absorption over all frequencies, and can be written as

$$\hat{\mu}_1 = 4k^3\left[-1+\left(e^{-kd}+2\sin kd\right)e^{-\mathrm{i}kd}\right]^{-1}, \tag{28a}$$

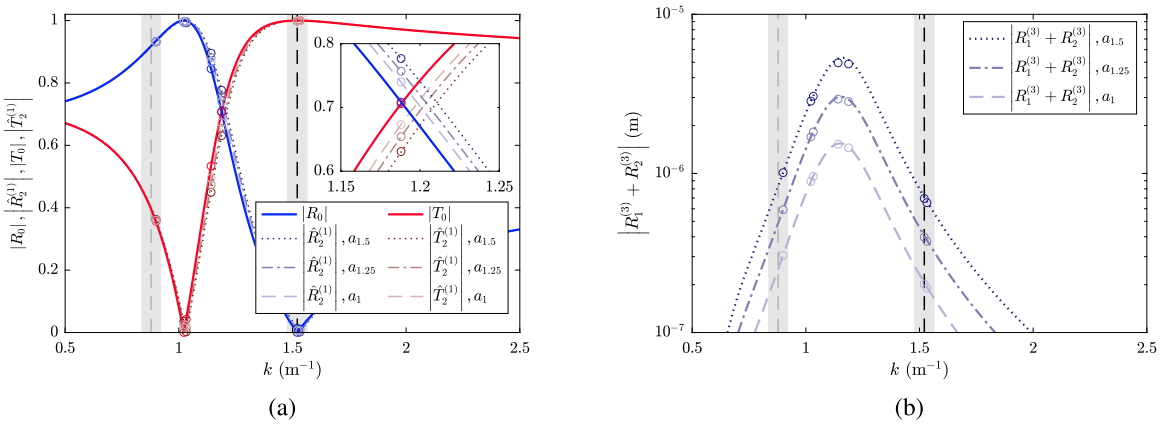

Fig. 3. (a) Leading-order reflection and transmission coefficients for a single scatterer (model B) with cubically nonlinear stiffness, also with higher-order corrections at the fundamental frequency for different incident amplitudes $a_j = j$ mm, $j = 1, 1.25, 1.5$. (b) Reflected amplitudes at the third harmonic for different incident amplitudes. The dashed vertical line corresponds to the linear resonance of the scatterer. The gray patches are centered around $k_n/\sqrt{3}$, where $k_n = 1.521$ m^{-1} is the resonance wavenumber of the scatterer. The circles correspond to FEM results.

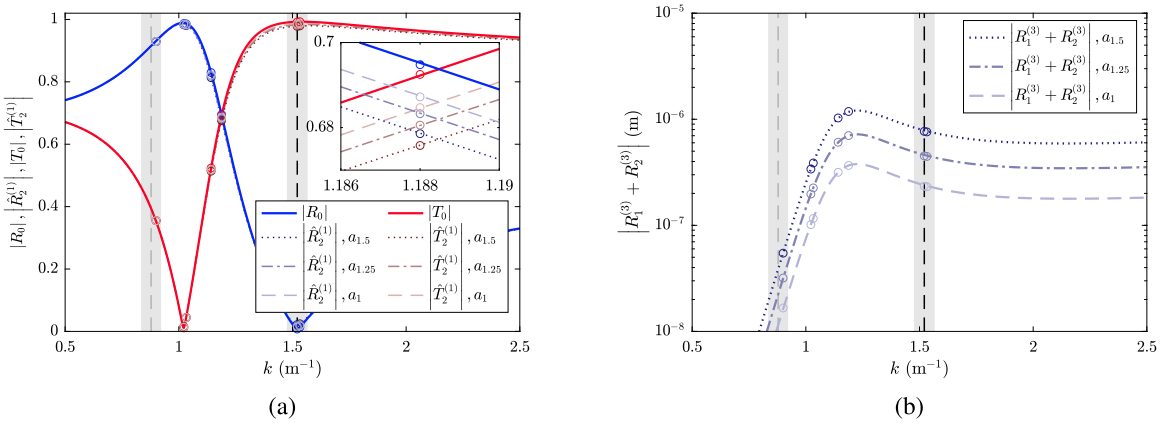

Fig. 4. (a) Leading-order reflection and transmission coefficients for a single scatterer (model B) with cubically nonlinear damping, also with higher-order corrections at the fundamental frequency for different incident amplitudes $a_j = j$ mm, $j = 1, 1.25, 1.5$. (b) Reflected amplitudes at the third harmonic for different incident amplitudes. The dashed vertical line corresponds to the resonance of the scatterer. The gray patches are centered around $k_n/\sqrt{3}$ and k_n, where $k_n = 1.521$ m^{-1} is the resonance wavenumber of the scatterer. The circles correspond to FEM results.

$$\hat{\mu}_2 = 4k^3 \left[-1 + e^{-kd} e^{ikd}\right]^{-1}, \tag{28b}$$

where d is the distance between the two scatterers. These impedances are both passive for $kd \in [1.0067\pi, 2\pi]$. We then seek a pair of mass–spring–damper scatterers of model A, whose impedance is given in Eq. (A.1), that achieve one-sided total absorption at a specific frequency, or equivalently, wavenumber. For this aim, we choose a value for $kd = k_0 d$ that lies within the range of the nondimensional wavenumber where the impedances of Eq. (28) are passive. By assuming given values for the distance between the scatterers, d, and the masses of the two scatterers, M_1, M_2, and equating the real and imaginary parts of each of Eqs. (28a) and (28b) with those of Eq. (A.1), all evaluated at k_0, we can extract the stiffness, $\hat{\kappa}_1, \hat{\kappa}_2$, and damping, $\hat{\nu}_1, \hat{\nu}_2$, coefficients of the two scatterers. We have thus designed a cluster of two mass–spring–damper scatterers of model A that completely absorb waves incident from the left with wavenumber k_0.

We then introduce a nonlinear stiffness with coefficient κ_2^* into the second scatterer, whereas the first scatterer remains linear ($\kappa_1^* = 0$). This nonlinear cluster will now not present total absorption at the specified wavenumber k_0, since the response at the fundamental will now be shifted by the higher-order contributions $R_n^{(1)}$ and $T_n^{(1)}$, given by Eqs. (22a) and (22b). To get a cluster that achieves total absorption at k_0 for a given incident amplitude a we choose to keep M_1 and M_2 unaltered and determine the value of κ_2^*, and we use a combined gradient- and genetic algorithm-based optimization approach to determine κ_1, κ_2, ν_1 and ν_2 that minimize the scattered power at the fundamental, given by $\left|R_+^{(1)}(k_0)\right|^2 + \left|T_+^{(1)}(k_0)\right|^2$, where $R_+^{(1)} = R_{0+} + (R_{1+}^{(1)} + R_{2+}^{(1)})/a$ and $T_+^{(1)} = T_0 + (T_{1+}^{(1)} + T_{2+}^{(1)})/a$. We expect that the response of minimum scattered power by the nonlinear cluster at the fundamental should occur at a wavenumber close to k_0, since the shift induced by the nonlinearity is expected to be small. The goal function

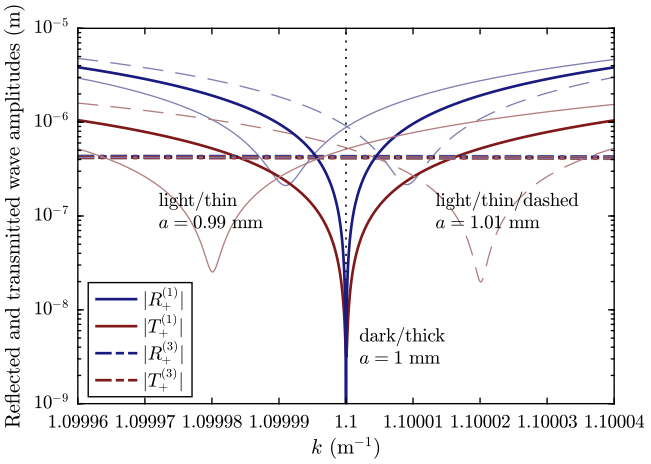

Fig. 5. Amplitude of the reflected and transmitted waves at the fundamental and at the third harmonic from a cluster of two scatterers with a wave incident from the left, for three different incident amplitudes. Model parameters are selected to give nearly total absorption of the fundamental frequency when the input amplitude is 1 mm. When the incident amplitude is slightly different from the optimal, the cluster ceases to perform as an absorbing filter, as seen by the reflected and transmitted amplitudes plotted in light-colored thin lines. The reflected and transmitted amplitudes at the third harmonic for all input amplitudes, plotted in dashed and dash-dotted lines, are practically indistinguishable from each other at the scaling of the graph.

of minimum scattered power at k_0 should then be achievable by a specific small perturbation of the free parameters with respect to those that give $\left|R_{0+}(k_0)\right|^2 + \left|T_0(k_0)\right|^2 = 0$, that is, perfect absorption, in the linear case. Therefore, as starting values for the optimization parameters κ_1, κ_2, ν_1 and ν_2 we use the values of the corresponding hatted parameters, $\hat{\kappa}_1$, $\hat{\kappa}_2$, $\hat{\nu}_1$ and $\hat{\nu}_2$, obtained for the linear cluster above.

Choosing $d = \pi$ m, $M_1 = M_2 = 1$ kg, $\kappa_2^* = 10^2$ N m^{-3} and $k_0 = 1.1$ m^{-1}, the values for the stiffness and damping coefficients obtained from the optimization for $a = 10^{-3}$ m are $\kappa_1 = 1.302778$ N m^{-1}, $\kappa_2 = 1.1367928$ N m^{-1}, $\nu_1 = 0.0478412$ N m^{-1} s^{-1} and $\nu_2 = 0.0019821$ N m^{-1} s^{-1}. A detail of the response of the system around k_0 for these values is given in Fig. 5 for three different input amplitudes, that is, the amplitude of $a = 10^{-3}$ m used for the optimization, a slightly smaller amplitude of 0.99×10^{-3} m and a slightly larger amplitude of 1.01×10^{-3} m. We first focus on the results for an input amplitude of 10^{-3} m, for which we get nearly perfect absorption at the fundamental frequency for $k = k_0$, in accordance with the optimization aim. It can be also seen that at this wavenumber, the generated third-harmonic waves are many orders of magnitude larger than those at the fundamental. We can also observe that this effect is very narrowband around k_0. If we then look into the response for the slightly non-optimal incident amplitudes of 0.99×10^{-3} and 1.01×10^{-3} m, plotted in lighter-colored lines, we can see that the scattered wave amplitudes at the fundamental at $k = k_0$ are now similar to or larger than those at the third harmonic, the latter being almost the same as those for the amplitude of 1×10^{-3} m. This means that the system presents a fine tuning with respect to the input amplitude, so that a wave incident from the left with wavenumber $k = k_0$ will be nearly fully absorbed only when its amplitude is very close to 1×10^{-3} m.

3.3.2. A frequency converter: three scatterers with transmission only at the third harmonic

We then present the design of a cluster of three scatterers of model *A* which receives the incident wave and only transmits the third harmonic. At the same time the reflection at the fundamental frequency may be arbitrary and the reflection at the third harmonic frequency is zero. A schematic of the system is illustrated in Fig. 6. We assume that either pair of consecutive scatterers are far away from each other, at least two wavelengths apart, so that we can neglect the effect of evanescent waves in the design procedure. To filter out the third harmonic from the reflection side and the fundamental from the transmission side we use linear, mass–spring outer scatterers and tune them to have zero transmission at the third harmonic and the fundamental, respectively, when in isolation. We then use a scatterer with a mass–spring–damper middle scatterer with nonlinear stiffness and optimize its linear stiffness coefficient to give a maximum third harmonic at $k = k_0$ when in isolation, given the other parameters of the scatterer. Finally, we choose an input amplitude a and use a genetic-algorithm-based optimization for the position of the middle scatterer to produce a maximum of the global third harmonic transmission coefficient of the cluster at $k = k_0$.

Results for $k_0 = 1.03$ m^{-1}, $\rho' = 1$ kg m^{-1}, $D = 1$ N m^2, $M_1 = M_2 = M_3 = 1$ kg, $\kappa_1 = 7.0052$ N m^{-1}, $\kappa_2 = 0.875$ N m^{-1}, $\kappa_3 = 0.895$ N m^{-1}, $\nu_1 = \nu_3 = 0$ N m^{-1} s^{-1}, $\nu_2 = 0.0187$ N m^{-1} s^{-1}, $\kappa_1^* = \kappa_3^* = 0$ N m^{-3}, $\kappa_2^* = 500$ N m^{-3}, $x_1 = 0$ m, $x_2 = 22.014$ m, $x_3 = 38.4311$ m, with $a = 1$ mm used for the optimization, are shown in Fig. 7 for three different incident amplitudes. It can be seen that at $k_0 = 1.03$ m^{-1} the transmission coefficient at the fundamental and the reflection coefficient at the third harmonic vanish, so that only a third-harmonic wave is transmitted, and only a fundamental-frequency wave is reflected. Therefore, this cluster acts as a frequency converter, transferring a portion of the incident energy to the third harmonic and transmitting it. It can also be seen that this effect is independent of incident amplitude, since the filtering at the two sides of the cluster is achieved with the outer, linear scatterers, whose response does not depend on amplitude.

The response of the frequency converter also clearly demonstrates the breaking of reciprocity, that is, the transmission differs depending on the side of incidence. A wave with $k = 1.03$ m^{-1} incident from the right is fully reflected by the first scatterer it

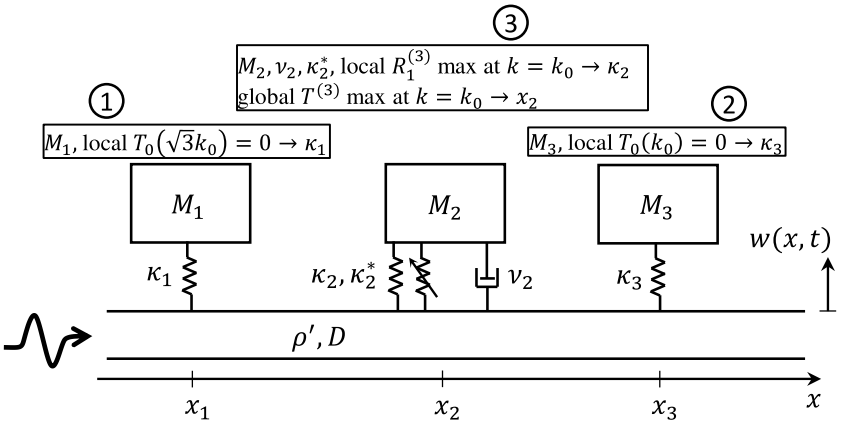

Fig. 6. Design of a cluster of three scatterers which transmits only the third harmonic when excited at a specific wavenumber k_0 for left incidence. Design steps: 0) assume scatterers of impedance model A, where the two outer ones are linear and lossless and the middle one also has linear damping and nonlinear stiffness. Also assume incidence from the left and that all scatterers are far enough from each other to avoid nearfield tunneling. 1) Choose M_1 and define κ_1 so that scatterer 1 locally does not transmit the third harmonic, so that this will not be reflected by the cluster. 2) Assume M_3 and define κ_3 so that scatterer 3 locally does not transmit the fundamental wavenumber, so that this will not be transmitted by the cluster. 3) Choose M_2, ν_2, κ_2^* and define κ_2 so that scatterer 2 generates a third harmonic with its maximum at around $k = k_0$. Choose an input amplitude a and optimize the position x_2 to give a maximum global transmitted third harmonic, $T^{(3)}$, at $k = k_0$.

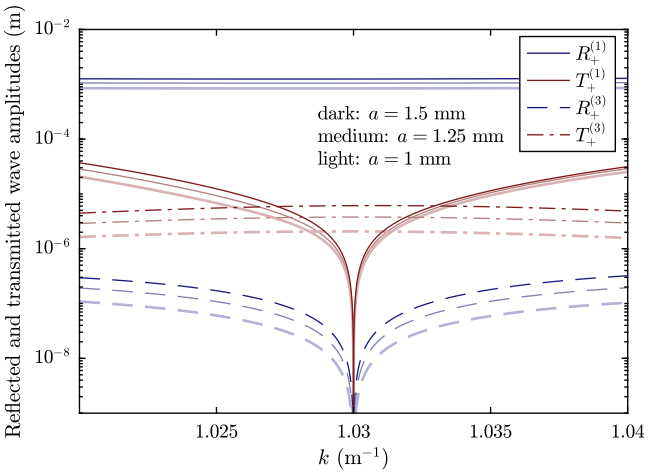

Fig. 7. Amplitude of the reflected and transmitted waves at the fundamental and at the third harmonic from a cluster of three scatterers with a wave incident from the left, designed according to the procedure outlined in Fig. 6 with the position of the middle scatterer optimized to give a maximum transmitted third harmonic at $k = 1.03$ m^{-1} when the input amplitude is 1 mm. Results for three different incident amplitudes are shown.

encounters, regardless of incident amplitude. Therefore, no third-harmonic wave will be produced, since the incident wave will not reach the middle, nonlinear scatterer. This presents an obvious asymmetry with the case of incidence from the left, where a considerable third-harmonic wave is generated, as seen in Fig. 7.

4. Conclusions

The multiple-scattering problem of flexural waves on a beam with nonlinear point attachments has been studied. Two particular types of mass–spring–damper scatterers have been considered, and two different types of nonlinearity, that is, nonlinear stiffness and nonlinear damping, both with a power-law dependence on the displacement and velocity, respectively. Analytical solutions for the vertical displacement of the beam have been obtained using a perturbation expansion with respect to a bookkeeping parameter. The perturbation expansion of the nonlinear equation of motion results in an infinite-ordered set of inhomogeneous linear equations, which are solved sequentially. The zeroth-order equation corresponds to the linear multiple-scattering problem, and the first-order solution needs to be considered to capture the effect of nonlinearity. Second-order approximations have been used in the presented results for higher accuracy.

The analysis of the nonlinear multiple-scattering problem leads to three fundamental differences as compared to the linear counterpart.

1. Harmonic waves at frequencies that are multiples of the incident wave are generated at a nonlinear scatterer. As a consequence, part of the incident energy is transferred from the fundamental to higher harmonic frequencies. These higher-harmonic waves undergo complex scattering between the attachments, which may be controlled by proper adjustment of the scatterers' impedances and positions.
2. The fundamental-frequency component admits an amplitude-dependent correction term at higher expansion orders. This correction term may be asymmetric with respect to the incidence side and affects the reflection and transmission coefficients, enabling (amplitude-)tunability of the dynamic characteristics of the system.
3. As a result of the two previous properties, when at least two scatterers are present, not only the reflection, but also the transmission at the different harmonics (including the fundamental) may be asymmetric with respect to the side of incidence. Therefore, the nonlinearity causes the system to behave non-reciprocally.

The proposed solution approach for the nonlinear multiple-scattering problem was first validated against FEM results for a single nonlinear scatterer of cubically nonlinear stiffness or damping for either of the two mass–spring–damper scatterer models. The cubic nonlinearity generates the third-harmonic component at the first expansion order, thus demonstrating energy conversion from the fundamental to the third harmonic, as well as a fundamental-frequency component that is superimposed with the incident wave. The complex amplitudes of both the third harmonic and the generated additional fundamental-frequency component depend on the incident wave amplitude. In the case of the third harmonic, this means that the third harmonic wave amplitude depends on the incident wave amplitude. For the fundamental frequency, it is shown that the amplitude-dependent "correction" generated by the nonlinearity renders the response of the scatterer tunable by controlling the incident amplitude. This can, for example, make it possible to shift the frequencies at which either the reflection or the transmission becomes minimum or maximum by controlling the amplitude of the incident wave.

Analytical results for two examples of attachment clusters which exhibit more complicated scattering patterns were next presented. The first setup consists of two scatterers where one has a cubically nonlinear spring. The system parameters are selected to nearly completely absorb the fundamental-frequency wave only at a specific incident amplitude for one side of incidence. Thus, the system behaves as an amplitude-tunable filter at a specific frequency. The second system consists or three scatterers where the middle one has cubically nonlinear spring. The cluster is designed to prevent transmission of the fundamental frequency and allow transmission of the third harmonic. Therefore, this system comprises a frequency converter, with a proportion of the incident energy transferred to the third harmonic along the direction of transmission, when the wave is incident from the left. This frequency converter also clearly illustrates the induced non-reciprocity, since if the input wave is incident from the right, no waves at the fundamental and third harmonic frequencies are transmitted.

The nonlinear multiple-scattering analysis framework developed here allows for investigation of the interaction between waves propagating in a linear substrate (beam) with nonlinear point attachments. The latter can be seen as a nonlinear point force, which depends on the beam displacement at that point. Such coupling is characteristic of a mechanical element interacting with the beam. Therefore, the proposed method can be applied to model, predict and control the response of point-contacts with Hertzian nonlinearity or finite deformation effects, mechanical joints with nonlinearity due to cracks, frictional attachments, and other common departures from purely linear behavior.

CRediT authorship contribution statement

Angelis Karlos: Methodology, Validation, Formal analysis, Writing – original draft. **Pawel Packo:** Conceptualization, Methodology, Validation, Formal analysis, Writing – original draft. **Andrew N. Norris:** Conceptualization, Methodology, Formal analysis, Writing – review & editing.

Declaration of competing interest

The authors declare that they have no known competing financial interests or personal relationships that could have appeared to influence the work reported in this paper.

Acknowledgments

A.K. and P.P. acknowledge support from the National Science Centre in Poland through Grant No. 2018/31/B/ST8/00753. A.N.N. acknowledges support from NSF USA, EFRI award no. 1641078.

Appendix A. Linear impedance models

Expressions are given for the complex impedance coefficients $\mu_{A\alpha}^{(m)}$, introduced in Eq. (8), for the two most popular discrete impedance models [5,12]. Models A and B can be achieved through parallel combinations of a spring and a damper attached to a mass.

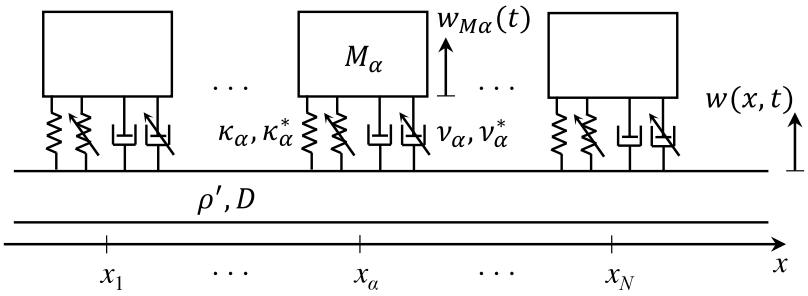

Fig. A.8. Schematic of an infinite beam of linear density ρ' and bending stiffness D with N model A scatterers. The αth scatterer, positioned at x_α, consists of a mass, M_α, connected to the beam via a spring of stiffness κ_α and a damper of damping coefficient ν_α. The stiffness and the damping can in general be nonlinear, with coefficients κ_α^* and ν_α^*.

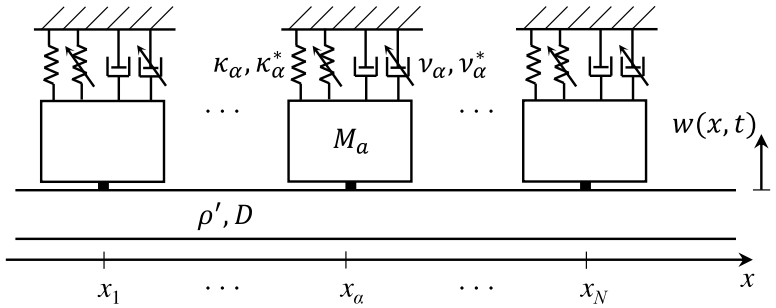

Fig. A.9. Schematic of an infinite beam of linear density ρ' and bending stiffness D with N point scatterers of impedance model B attached to it, where the αth scatterer, positioned at x_α, consists of a mass, M_α, clamped on the beam and connected to a rigid constraint through a spring of stiffness κ_α and a damper of damping coefficient ν_α. The stiffness and the damping can in general be nonlinear, with coefficients κ_α^* and ν_α^*.

A.1. Model A

Model A, denoted μ_A, has a mass, M_α, connected to the beam at position x_α via a parallel combination of a spring of stiffness κ_α and a damper of damping coefficient ν_α, as shown in the middle of Fig. A.8 (the spring and damper with arrows denote nonlinear elements, not considered in this section). The impedance of the αth scatterer, $\mu_{A\alpha}$, is defined as the ratio of the scatterer force acting on the beam, to the displacement of the beam at the attachment, and, in general for the mth harmonic frequency, is [5]

$$\mu_{A\alpha}^{(m)} = \frac{1}{D}\left(\frac{1}{(m\omega)^2 M_\alpha} - \frac{1}{\kappa_\alpha - \mathrm{i}(m\omega)\nu_\alpha}\right)^{-1}. \tag{A.1}$$

A.2. Model B

Model B is a point mass clamped to the beam and connected to a rigid constraint through a parallel connection of a spring and a damper, as shown in Fig. A.9. The impedance for this scatterer for the mth harmonic frequency, which stems from its linear properties, is expressed as [5]

$$\mu_{B\alpha}^{(m)} = \frac{1}{D}\left((m\omega)^2 M_\alpha + \mathrm{i}\,(m\omega)\,\nu_\alpha - \kappa_\alpha\right). \tag{A.2}$$

Appendix B. Nonlinear forcing terms

B.1. Models A and B

The forcing terms for quadratic and cubic nonlinearity for an arbitrary expansion order, both for nonlinear stiffness and nonlinear damping, are given here. For notational convenience, we present the following analysis in terms of the nth-order displacement, w_n, which is sufficient for impedance model B, where no additional degree of freedom is present (i.e. $w'_\alpha(\tau) = 0$). The same procedure

can be followed for impedance model A using the displacement difference $w_n - w_{Mn}$ (then $w'_\alpha(\tau) = w_{Mn}$). It can be seen from Eqs. (2)–(4) and (A.2) that the nonlinear stiffness and damping terms can be written as

$$\sum_{n=1}^{\infty} \epsilon^n C_n = \sum_{n=1}^{\infty} \epsilon^n \left(S_n + D_n\right) = -\epsilon \frac{\kappa^*}{D} \left(\sum_{n=0}^{\infty} \epsilon^n w_n\right)^p - \epsilon \frac{\nu^*}{D} \left(\sum_{n=0}^{\infty} \epsilon^n \dot{w}_n\right)^p, \tag{B.1}$$

for a generic nonlinearity of order p. Terms S_n and D_n in (B.1) stand for the stiffness- and damping-induced nonlinear forces, respectively. This form of nonlinear forcing is next specified for the quadratic and cubic nonlinearities. Note that the dimensions/units of κ^* and ν^* depend upon p and the fact that C_n has dimensions of (length)$^{-2}$.

B.1.1. Model A

Impedance model A involves an additional degree of freedom as compared to model B, that is, the displacement of the scatterer mass. Some elaboration is therefore required to obtain the forcing terms $c_n^{(m)}$ in Eq. (14). By expanding the equation of motion of the mass, the mass displacement amplitude of order n and at harmonic $m\omega$ can be written with respect to the corresponding beam displacement amplitude and the forcing terms as

$$u_{Mn}^{(m)} = \frac{\mu_{SD}^{(m)}}{\mu_M^{(m)} + \mu_{SD}^{(m)}} u_n^{(m)} + \frac{s_n^{(m)} + d_n^{(m)}}{\mu_M^{(m)} + \mu_{SD}^{(m)}}, \tag{B.2}$$

where

$$\mu_M^{(m)} = \frac{1}{D}(m\omega)^2 M, \quad \mu_{SD}^{(m)} = \frac{1}{D}\left(\mathrm{i}m\omega\nu - \kappa\right), \tag{B.3}$$

and $s_n^{(m)}$ and $d_n^{(m)}$ are functions of the displacement difference of the beam and the scatterer mass, $u_n^{(m)} - u_M^{(m)}$ (instead of only the beam displacement $u_n^{(m)}$ in the simpler model B below). It is also recalled that the beam displacement is evaluated at the scatterer's position. The nth-order and mth-harmonic force acting on the beam, which corresponds to the bracketed term in the sum in Eq. (14), is written as

$$\mu_M^{(m)} u_{Mn}^{(m)} = \mu_A^{(m)} u_n^{(m)} + \frac{\mu_A^{(m)}}{\mu_{SD}^{(m)}} \left(s_n^{(m)} + d_n^{(m)}\right), \tag{B.4}$$

where the impedance of model A, given in Eq. (A.1), has been expressed as $\mu_A^{(m)} = \mu_M^{(m)} \mu_{SD}^{(m)} / (\mu_M^{(m)} + \mu_{SD}^{(m)})$. Consequently, the forcing terms $c_n^{(m)}$ in Eq. (14) for impedance model A are given by

$$c_n^{(m)} = \frac{\mu_A^{(m)}}{\mu_{SD}^{(m)}} \left(s_n^{(m)} + d_n^{(m)}\right). \tag{B.5}$$

B.1.2. Model B

For impedance model B, where the beam displacement is the only degree of freedom present, the forcing terms $c_n^{(m)}$ in Eq. (14) are

$$c_n^{(m)} = s_n^{(m)} + d_n^{(m)}, \tag{B.6}$$

where $s_n^{(m)}$ and $d_n^{(m)}$ are related to S_n and D_n via

$$\begin{aligned} S_n &= \frac{1}{2} \sum_m s_n^{(m)} e^{-\mathrm{i}m\tau} + \text{c.c.}, \\ D_n &= \frac{1}{2} \sum_m d_n^{(m)} e^{-\mathrm{i}m\tau} + \text{c.c.}. \end{aligned} \tag{B.7}$$

Explicit expressions for $s_n^{(m)}$ and $d_n^{(m)}$ for $n = 1$ and $n = 2$ for quadratic and cubic nonlinearity for impedance model B are given next.

B.2. Quadratic nonlinearity

We first consider the forcing due to the nonlinear stiffness, S_n, which only involves the first term in the right-hand side of Eq. (B.1). For quadratic nonlinearity, $p = 2$, the square of the sum can be expressed as a Cauchy product, giving

$$\sum_{n=1}^{\infty} \epsilon^n S_n = -\epsilon \frac{\kappa^*}{D} \sum_{n=0}^{\infty} \epsilon^n \sum_{j=0}^{n} w_j w_{n-j} \Rightarrow \sum_{n=1}^{\infty} \epsilon^n S_n = -\frac{\kappa^*}{D} \sum_{n=1}^{\infty} \epsilon^n \sum_{j=0}^{n-1} w_j w_{n-1-j}. \tag{B.8}$$

It follows from Eq. (B.8) that

$$S_n = -\frac{\kappa^*}{D} \sum_{j=0}^{n-1} w_j w_{n-1-j}. \tag{B.9}$$

The calculation of S_n requires the n displacements of previous expansion orders from zero to $n-1$, calling for a sequential solution procedure. Starting from ϵ^1 and expressing the displacements w_0 as in Eq. (7), S_1 is written as

$$S_1 = -\frac{\kappa^*}{D} w_0^2 = -\frac{\kappa^*}{D}\left(\frac{1}{2}u_0 e^{-\mathrm{i}\tau} + \mathrm{c.c.}\right)^2 = -\frac{1}{4}\frac{\kappa^*}{D}\left(|u_0|^2 + u_0^2 e^{-\mathrm{i}2\tau} + \mathrm{c.c.}\right), \tag{B.10}$$

where all terms are evaluated at x_α. It can be seen that the forcing term S_1 involves a zero-frequency (DC) and 2ω terms. Consequently, the terms of these time-dependent factors will appear in the first-order displacement as

$$w_1 = \frac{1}{2}u_1^{(0)} + \frac{1}{2}u_1^{(2)} e^{-\mathrm{i}2\tau} + \mathrm{c.c.}. \tag{B.11}$$

With this, the second-order quadratic forcing term can be derived as

$$S_2 = -2\frac{\kappa^*}{D} w_0 w_1 = -\frac{1}{2}\frac{\kappa^*}{D}\left[\left(2u_0 \mathrm{Re}\left\{u_1^{(0)}\right\} + \bar{u}_0 u_1^{(2)}\right) e^{-\mathrm{i}\tau} + u_0 u_1^{(2)} e^{-\mathrm{i}3\tau} + \mathrm{c.c.}\right]. \tag{B.12}$$

Eq. (B.12) shows that the second-order displacement will involve wave components at frequencies ω and 3ω, and can therefore be written as

$$w_2 = \frac{1}{2}u_2^{(1)} e^{-\mathrm{i}\tau} + \frac{1}{2}u_2^{(3)} e^{-\mathrm{i}3\tau} + \mathrm{c.c.}. \tag{B.13}$$

In the same way, S_3 can be calculated, which will involve a DC term and harmonics at 2ω and 4ω. In general, it can be deduced from the form of the forcing terms S_n given in Eq. (B.9) for quadratic nonlinearity that the nth-order forcing term will involve all the odd or even harmonics up to order $n+1$ for n even or odd, respectively. Therefore, the terms S_n can be expressed with respect to forcing terms $s_n^{(m)}$ corresponding to the nth-order wave amplitudes at frequency $m\omega$ as

$$S_n = \begin{cases} \frac{1}{2}\sum_{j=0}^{\frac{n}{2}} s_n^{(2j+1)} e^{-\mathrm{i}(2j+1)\tau} + \mathrm{c.c.}, & \text{for } n \text{ even}, \\ \frac{1}{2}\sum_{j=0}^{\frac{n+1}{2}} s_n^{(2j)} e^{-\mathrm{i}2j\tau} + \mathrm{c.c.}, & \text{for } n \text{ odd}. \end{cases} \tag{B.14}$$

For the equations of orders ϵ^1 and ϵ^2, for which S_n is written explicitly in Eqs. (B.10) and (B.12), the forcing terms $s_n^{(m)}$ for the wave amplitudes can be derived by comparison with the appropriate branch of Eq. (B.14) for n either odd or even, which gives

$$\begin{aligned} s_1^{(0)} &= -\frac{1}{2}\frac{\kappa^*}{D}|u_0|^2, \quad s_1^{(2)} = -\frac{1}{2}\frac{\kappa^*}{D}u_0^2, \\ s_2^{(1)} &= -\frac{\kappa^*}{D}\left(2u_0 \mathrm{Re}\left\{u_1^{(0)}\right\} + \bar{u}_0 u_1^{(2)}\right), \quad s_2^{(3)} = -\frac{\kappa^*}{D}u_0 u_1^{(2)}. \end{aligned} \tag{B.15}$$

Next, we consider the forcing term D_n due to nonlinear damping of power-law dependence on the velocity, for which Eq. (B.1) gives

$$\sum_{n=1}^{\infty} \epsilon^n D_n = -\epsilon \frac{\nu^*}{D}\left(\sum_{n=0}^{\infty} \epsilon^n \dot{w}_n\right)^p. \tag{B.16}$$

The forcing terms are then given by

$$D_n = -\frac{\nu^*}{D}\sum_{j=0}^{n-1} \dot{w}_j \dot{w}_{n-1-j}. \tag{B.17}$$

Following the same procedure as above, but using the time derivatives of the displacements, gives the complex forcing terms, $d_n^{(m)}$, for the first two higher orders of expansion as

$$\begin{aligned} d_1^{(0)} &= -\frac{1}{2}\frac{\kappa^*}{D}\omega^2|u_0|^2, \quad d_1^{(2)} = \frac{1}{2}\frac{\kappa^*}{D}\omega^2 u_0^2, \\ d_2^{(1)} &= -2\frac{\kappa^*}{D}\omega^2 \bar{u}_0 u_1^{(2)}, \quad d_2^{(3)} = 2\frac{\kappa^*}{D}\omega^2 u_0 u_1^{(2)}. \end{aligned} \tag{B.18}$$

For impedance model A, the forcing terms can be calculated from Eqs. (B.15) and (B.18) if instead of the beam displacement $u_j^{(m)}$, $j < n$, the displacement difference $u_j^{(m)} - u_{Mj}^{(m)}$ is used, where $u_{Mj}^{(m)}$ is the mass displacement amplitude, calculated with Eq. (B.2). At the zeroth order, the nonlinear forcing terms are zero, so that Eq. (B.2) reduces to $u_{Mn}^{(m)} = \mu_M^{(m)} u_n^{(m)} / (\mu_M^{(m)} + \mu_{SD}^{(m)})$.

B.3. Cubic nonlinearity

For cubic nonlinearity, the nonlinear stiffness forcing terms S_n are again found by expressing the series raised to the power $p = 3$ in Eq. (B.1) using Cauchy products, which gives

$$S_n = -\frac{\kappa^*}{D}\sum_{j=0}^{n-1}\sum_{l=0}^{n-1-j} w_j w_{n-1-j-l} w_l. \tag{B.19}$$

For $n = 1$ and $n = 2$, this gives, respectively,

$$S_1 = -\frac{\kappa^*}{D} w_0^3 = -\frac{\kappa^*}{8D}\left(3u_0|u_0|^2 e^{-\mathrm{i}\tau} + u_0^3 e^{-\mathrm{i}3\tau} + \mathrm{c.c.}\right), \tag{B.20a}$$

$$S_2 = -\frac{\kappa^*}{D} 3w_0^2 w_1 = -\frac{3\kappa^*}{8D}\Big(\left(u_0^2 \bar{u}_1^{(1)} + \bar{u}_0^2 u_1^{(3)} + 2\left|u_0\right|^2 u_1^{(1)}\right) e^{-\mathrm{i}\tau} + \left(u_0^2 u_1^{(1)} + 2\left|u_0\right|^2 u_1^{(3)}\right) e^{-\mathrm{i}3\tau} + u_0^2 u_1^{(3)} e^{-\mathrm{i}5\tau} + \text{c.c.}\Big), \tag{B.20b}$$

where w_0 is expressed as

$$w_0 = \frac{1}{2} u_0 e^{-\mathrm{i}\tau} + \text{c.c.}, \tag{B.21}$$

and w_1 is defined as

$$w_1 = \frac{1}{2} u_1^{(1)} e^{-\mathrm{i}\tau} + \frac{1}{2} u_1^{(3)} e^{-\mathrm{i}3\tau} + \text{c.c.}, \tag{B.22}$$

to account for the fact that S_1 has components at ω and at 3ω. In general, it can be deduced from the form of the forcing terms S_n for cubic nonlinearity as given in Eq. (B.19) that these involve all the odd-order harmonics from 1 up to $2n+1$, as can be seen for the first two orders in Eqs. (B.20a) and (B.20b). Therefore, S_n can be expressed with respect to the forcing terms $s_n^{(m)}$ for the nth-order wave amplitudes at frequencies $n\omega$ as

$$S_n = \frac{1}{2} \sum_{j=0}^{n} s_n^{(2j+1)} e^{-\mathrm{i}(2j+1)\tau} + \text{c.c.}, \tag{B.23}$$

which in this case holds for n either odd or even. It can thus be deduced that no DC term or even-order harmonics are generated with a cubic nonlinearity. For the equations of orders 1 and 2, the forcing terms $s_n^{(m)}$ can be found by comparing Eqs. (B.20a) and (B.20b) with Eq. (B.23), giving

$$\begin{aligned} s_1^{(1)} &= -\frac{3}{4}\frac{\kappa^*}{D} u_0 \left|u_0\right|^2, \quad s_1^{(3)} = -\frac{1}{4}\frac{\kappa^*}{D} u_0^3, \\ s_2^{(1)} &= -\frac{3}{4}\frac{\kappa^*}{D}\left(u_0^2 \bar{u}_1^{(1)} + \bar{u}_0^2 u_1^{(3)} + 2\left|u_0\right|^2 u_1^{(1)}\right), \\ s_2^{(3)} &= -\frac{3}{4}\frac{\kappa^*}{D}\left(u_0^2 u_1^{(1)} + 2\left|u_0\right|^2 u_1^{(3)}\right), \quad s_2^{(5)} = -\frac{3}{4}\frac{\kappa^*}{D} u_0^2 u_1^{(3)}. \end{aligned} \tag{B.24}$$

For nonlinear damping, where Eq. (B.16) holds, the real forcing terms are given by

$$D_n = -\frac{\nu^*}{D} \sum_{j=0}^{n-1} \sum_{l=0}^{n-1-j} \dot{w}_j \dot{w}_{n-1-j-l} \dot{w}_l, \tag{B.25}$$

which gives the complex forcing terms, $d_n^{(m)}$, for the first two higher orders of expansion as

$$\begin{aligned} d_1^{(1)} &= \mathrm{i}\frac{3}{4}\frac{\nu^*}{D}\omega^3 u_0 \left|u_0\right|^2, \quad d_1^{(3)} = -\frac{\mathrm{i}}{4}\frac{\nu^*}{D}\omega^3 u_0^3, \\ d_2^{(1)} &= \mathrm{i}\frac{3}{4}\frac{\nu^*}{D}\omega^3\left(2\left|u_0\right|^2 u_1^{(1)} - 3\bar{u}_0^2 u_1^{(3)} + u_0^2 \bar{u}_1^{(1)}\right), \\ d_2^{(3)} &= \mathrm{i}\frac{3}{4}\frac{\nu^*}{D}\omega^3\left(6\left|u_0\right|^2 u_1^{(3)} - u_0^2 u_1^{(1)}\right), \quad d_2^{(5)} = -\mathrm{i}\frac{9}{4}\frac{\nu^*}{D}\omega^3 u_0^2 u_1^{(3)}. \end{aligned} \tag{B.26}$$

As in the case of quadratic nonlinearity, the forcing terms for impedance model A can be calculated from Eqs. (B.26) if the displacement difference $u_j^{(m)} - u_{Mj}^{(m)}$ is used instead of $u_j^{(m)}$, $j < n$, also using Eq. (B.2) for the mass amplitude.

References

[1] A. Merkel, G. Theocharis, O. Richoux, V. Romero-García, V. Pagneux, Control of acoustic absorption in one-dimensional scattering by resonant scatterers, Appl. Phys. Lett. 107 (24) (2015) 244102, http://dx.doi.org/10.1063/1.4938121.

[2] J. Ormondroyd, J. Den Hartog, The theory of the dynamical vibration absorber, ASME J. Appl. Mech. 50 (1928) 9–22.

[3] M. Brennan, Control of flexural waves on a beam using a tunable vibration neutraliser, J. Sound Vib. 222 (3) (1999) 389–407, http://dx.doi.org/10.1006/jsvi.1998.2031.

[4] H. El-Khatib, B. Mace, M. Brennan, Suppression of bending waves in a beam using a tuned vibration absorber, J. Sound Vib. 288 (4) (2005) 1157–1175, http://dx.doi.org/10.1016/j.jsv.2005.01.024.

[5] A.N. Norris, P. Packo, Non-symmetric flexural wave scattering and one-way extreme absorption, J. Acoust. Soc. Am. 146 (1) (2019) 873–883, http://dx.doi.org/10.1121/1.5087133.

[6] M. Yang, C. Meng, C. Fu, Y. Li, Z. Yang, P. Sheng, Subwavelength total acoustic absorption with degenerate resonators, Appl. Phys. Lett. 107 (10) (2015) 104104, http://dx.doi.org/10.1063/1.4930944.

[7] J. Achenbach, Reciprocity in Elastodynamics, Cambridge University Press, Cambridge, UK, 2004.

[8] M. Brennan, Vibration control using a tunable vibration neutralizer, Proc. Inst. Mech. Eng. C J. Mech. Eng. Sci. 211 (2) (1997) 91–108, http://dx.doi.org/10.1243/0954406971521683.

[9] P. Gardonio, M. Zilletti, Integrated tuned vibration absorbers: A theoretical study, J. Acoust. Soc. Am. 134 (5) (2013) 3631–3644, http://dx.doi.org/10.1121/1.4824123.

[10] A. Nayfeh, D. Mook, Nonlinear Oscillations, in: Wiley Classics Library, Wiley, 2008.

[11] P. Packo, T. Uhl, W.J. Staszewski, M.J. Leamy, Amplitude-dependent lamb wave dispersion in nonlinear plates, J. Acoust. Soc. Am. 140 (2) (2016) 1319–1331, http://dx.doi.org/10.1121/1.4961489.

[12] D. Evans, R. Porter, Penetration of flexural waves through a periodically constrained thin elastic plate in vacuo and floating on water, J. Eng. Math. 58 (2007) 317–337, http://dx.doi.org/10.1007/s10665-006-9128-0.

[13] C. Wang, Z. Tay, Very large floating structures: Applications, research and development, Procedia Eng. 14 (2011) 62–72, http://dx.doi.org/10.1016/j.proeng.2011.07.007, The Proceedings of the Twelfth East Asia-Pacific Conference on Structural Engineering and Construction.
[14] C. Zhang, J. Achenbach, Effective wave velocity and attenuation in a material with distributed penny-shaped cracks, Int. J. Solids Struct. 27 (6) (1991) 751–767, http://dx.doi.org/10.1016/0020-7683(91)90032-B.
[15] P. Blanloeuil, A. Meziane, A. Norris, C. Bacon, Analytical extension of finite element solution for computing the nonlinear far field of ultrasonic waves scattered by a closed crack, Wave Motion 66 (2016) 132–146, http://dx.doi.org/10.1016/j.wavemoti.2016.04.016.
[16] S.B. Platts, N.V. Movchan, R.C. McPhedran, A.B. Movchan, Two-dimensional phononic crystals and scattering of elastic waves by an array of voids, Proc. Math. Phys. Eng. Sci. 458 (2002) 2327–2347.
[17] S. Hirsekorn, The scattering of ultrasonic waves by polycrystals, J. Acoust. Soc. Am. 72 (3) (1982) 1021–1031, http://dx.doi.org/10.1121/1.388233.
[18] A. Meziane, A.N. Norris, A.L. Shuvalov, Nonlinear shear wave interaction at a frictional interface: Energy dissipation and generation of harmonics, J. Acoust. Soc. Am. 130 (4) (2011) 1820–1828, http://dx.doi.org/10.1121/1.3628663.
[19] J. Qu, L.J. Jacobs, P.B. Nagy, On the acoustic-radiation-induced strain and stress in elastic solids with quadratic nonlinearity (L), J. Acoust. Soc. Am. 129 (6) (2011) 3449–3452, http://dx.doi.org/10.1121/1.3583501.